

# Stable and Steerable Sparse Autoencoders with Weight Regularization

Piotr Jedryszek  
 Department of Biology  
 University of Oxford, Oxford, UK  
 piotr.jedryszek@sjc.ox.ac.uk

Oliver M. Crook  
 Kavli Institute for Nanoscience Discovery,  
 Department of Chemistry  
 University of Oxford, Oxford, UK  
 oliver.crook@chem.ox.ac.uk

## Abstract

Sparse autoencoders (SAEs) are widely used to extract human-interpretable features from neural network activations, but their learned features can vary substantially across random seeds and training choices. To improve stability, we studied *weight regularization* by adding L1 or L2 penalties on encoder and decoder weights, and evaluate how regularization interacts with common SAE training defaults. On MNIST, we observe that L2 weight regularization produces a core of highly aligned features and, when combined with tied initialization and unit-norm decoder constraints, it dramatically increases cross-seed feature consistency. For TopK SAEs trained on language model activations (Pythia-70M-deduped), adding a small L2 weight penalty increased the fraction of features shared across three random seeds and roughly doubles steering success rates, while leaving the mean of automated interpretability scores essentially unchanged. Finally, in the regularized setting, activation steering success becomes better predicted by auto-interpretability scores, suggesting that regularization can align text-based feature explanations with functional controllability.

## 1 Introduction

Sparse autoencoders (SAEs) have become central to mechanistic interpretability, offering a potential solution to the superposition hypothesis, the idea that neural networks represent more features than dimensions by encoding them in overlapping patterns (Nelson Elhage et al., 2022). By learning an overcomplete basis with sparse coefficients, SAEs aim to recover the “true” features underlying model computations (Trenton Bricken et al., 2023; Cunningham et al., 2023). Despite their success, recent work raised concerns about SAE reliability. Chanin and Garriga-Alonso (2025) showed that SAE features are highly sensitive to the L0 sparsity hyperparameter, and (Gonçalo Paulo and Nora Belrose, 2025) demonstrated that SAEs trained with different random seeds on identical data learn substantially different features. This variability suggests **underconstrained optimization**: activation sparsity alone does not uniquely determine a solution.

This underdetermination may help explain mixed downstream results: in a large-scale study of activation probing, Kantamneni et al. (2025) find that SAE-based probes do not provide a consistent advantage over strong baselines on raw activations across several challenging regimes, although they sometimes outperform on individual datasets. Recent work also argues that SAE objectives should prioritize *functional faithfulness* to model behavior rather than reconstruction alone; that is, by training SAEs end-to-end to preserve model outputs (Braun et al., 2024). Other related work has begun to address these challenges by adding additional structure to SAE training beyond activation sparsity. For example, Marks et al. (2024) propose *Mutual Feature Regularization*, which trains multiple SAEs in parallel and encourages them to converge to similar features, motivated by the idea that features replicated across runs are more likely to correspond to genuine

input factors. Similarly, recently [Martin-Linares and Ling \(2025\)](#) introduced Distilled Matryoshka Sparse Autoencoders (DMSAEs), which run iterative train-and-select cycles: after each training run, features are scored by their gradient $\times$ activation contribution to next-token loss, and only the highest-attribution subset is carried forward as frozen encoder directions for the next cycle. Where Mutual Feature Regularization encourages convergence across *parallel* SAEs, DMSAEs enforce consistency across *sequential* retraining cycles.

In classical machine learning, underdetermined problems are addressed through **regularization**: additional constraints encoding prior beliefs about desirable solutions ([Ian Goodfellow et al., 2016](#)). L1 regularization (Laplace prior) encourages weight sparsity, while L2 regularization (Gaussian prior) encourages small, smoothly distributed weights. Both improve generalization in many settings ([Tibshirani, 1996](#); [Krizhevsky et al., 2012](#)).

In this work we revisit a simple idea: add an explicit weight penalty to SAE training, in addition to the usual activation sparsity term. We focus on three questions:

1. **Cross-seed consistency:** Does weight regularization increase the reproducibility of features across random seeds?
2. **Feature quality:** Does weight regularization affect downstream evaluations such as interpretability and steering?
3. **Interaction with SAE design choices:** How does weight regularization interact with common architectural and training decisions such as encoder/decoder initialization, decoder constraints, sparsity mechanism (TopK, BatchTopK, Matryoshka)?

We explore weight regularization first on a toy model of MNIST images to build intuitions, then on a small language model (Pythia-70M-deduped) to test real-world applicability.

## 2 Methods

### 2.1 Sparse autoencoders with weight regularization

Given an activation vector  $x \in \mathbb{R}^d$ , an SAE produces a sparse latent  $z \in \mathbb{R}^m$  and a reconstruction  $\hat{x}$ :

$$z = f(W_{\text{enc}}x + b_{\text{enc}}), \tag{1}$$

$$\hat{x} = W_{\text{dec}}z + b_{\text{dec}}. \tag{2}$$

We consider standard sparsity mechanisms for  $z$  (e.g. an explicit  $l_1$  penalty or a hard TopK constraint) and add weight regularization:

$$\mathcal{L} = \mathcal{L}_{\text{recon}}(x, \hat{x}) + \lambda_{\text{sparse}} \mathcal{L}_{\text{sparse}}(z) + \lambda_{\text{w}} \left( \|W_{\text{enc}}\|_p^p + \|W_{\text{dec}}\|_p^p \right), \quad p \in \{1, 2\}. \tag{3}$$

where  $\mathcal{L}_{\text{recon}}(x, \hat{x}) = \|x - \hat{x}\|_2^2$  is the mean squared error reconstruction loss. For TopK models, sparsity is enforced by the encoder and we set  $\mathcal{L}_{\text{sparse}}(z) = 0$ . Some implementations use mean rather than sum reductions (e.g.  $\text{mean}(|z|)$  or  $\text{mean}(|W|)$ ); though, for fixed layer shapes this differs by a constant factor that can be absorbed into  $\lambda_{\text{sparse}}$  or  $\lambda_{\text{w}}$ .

### 2.2 Decoder constraints and tied initialization

Two implementation choices are common in recent SAE work and are present in the default SAE implementations of SAEBench:

1. **Tied initialization:** initialize  $W_{\text{dec}} \leftarrow W_{\text{enc}}^\top$  so that each latent starts as an approximately self-consistent “detector” and “writer” direction.
2. **Unit-norm decoder columns:** enforce  $\|W_{\text{dec}}(:, i)\|_2 = 1$  for each decoder column via normalization during training.

A unit-norm constraint can neutralize L2 shrinkage on the decoder (since  $\|W_{\text{dec}}\|_F^2$  becomes constant), so the same  $\lambda_w$  may behave differently depending on whether decoder normalization is applied. Motivated by this, we explore these choices in a toy MNIST setting and retain SAEbench defaults when moving to language-model activations. Importantly, when unit-norm decoder columns are enforced,  $\|W_{\text{dec}}\|_F^2$  is constant and the weight penalty acts primarily as encoder regularization; the decoder L2 term contributes little beyond what the norm constraint already imposes.

### 2.3 Cross-seed feature consistency

To quantify reproducibility, we followed [Gonalo Paulo and Nora Belrose \(2025\)](#) and measured feature similarity across SAEs trained with different random seeds. For two trained SAEs  $A$  and  $B$ , let  $D_A, D_B \in \mathbb{R}^{m \times d}$  be the decoder feature matrices. We compute the absolute cosine similarity matrix  $S = |\cos(D_A, D_B)|$  and use Hungarian matching to obtain a one-to-one pairing. We report:

- **Mean max cosine:** average over features of  $\max_j S_{ij}$  (symmetrized across both directions).
- **Fraction paired:** fraction of features with  $\max_j S_{ij} > 0.7$ .
- **Shared features:** a stricter criterion requiring that the encoder and decoder Hungarian matchings agree *and* both matched similarities exceed 0.7 (sign-invariant).

### 2.4 Steering and evaluation

For language-model SAEs, we evaluated *feature steering* by injecting a decoder feature vector into the residual stream during text generation:

$$r_t \leftarrow r_t + \alpha d_i, \tag{4}$$

where  $d_i$  is decoder feature  $i$  and  $\alpha$  is the steering strength. We explored several strength parameterizations: fixed, residual-RMS scaled, and target pre-activation delta. The configuration yielding the best results for both regularized and unregularized SAEs used non-deterministic decoding (temperature = 0.7, top- $p$  = 0.9) with generation-only steering and fixed scaling ( $\alpha = 5$ ). Full hyperparameter details appear in [Appendix A](#).

An LLM judge (GPT-5.1) scored whether the steered output (completing a set of 5 prompts) was more related to the feature’s expected concept than the unsteered output on a 1–5 scale (5 = steered is much more related, 3 = no meaningful change, 1 = steered is much less related). We counted scores greater than or equal to four as successful steering.

## 3 Toy experiments on MNIST

### 3.1 Weight regularization induces an “aligned core”

We trained SAEs on flattened MNIST images ( $d = 784$ ) with  $m = 1,568$  latents ( $2 \times$  overcomplete) and an L1 sparsity penalty on activations. With untied initialization, adding L2 regularization ( $\lambda_w = 10^{-3}$ ) produced a bimodal distribution of encoder–decoder cosine similarities and yielded a small set of aligned features that qualitatively correspond to clean strokes and curves ([Figure 1](#)). A small number of high-cosine similarity latents accounted for most reconstruction capacity ([Appendix B](#)).

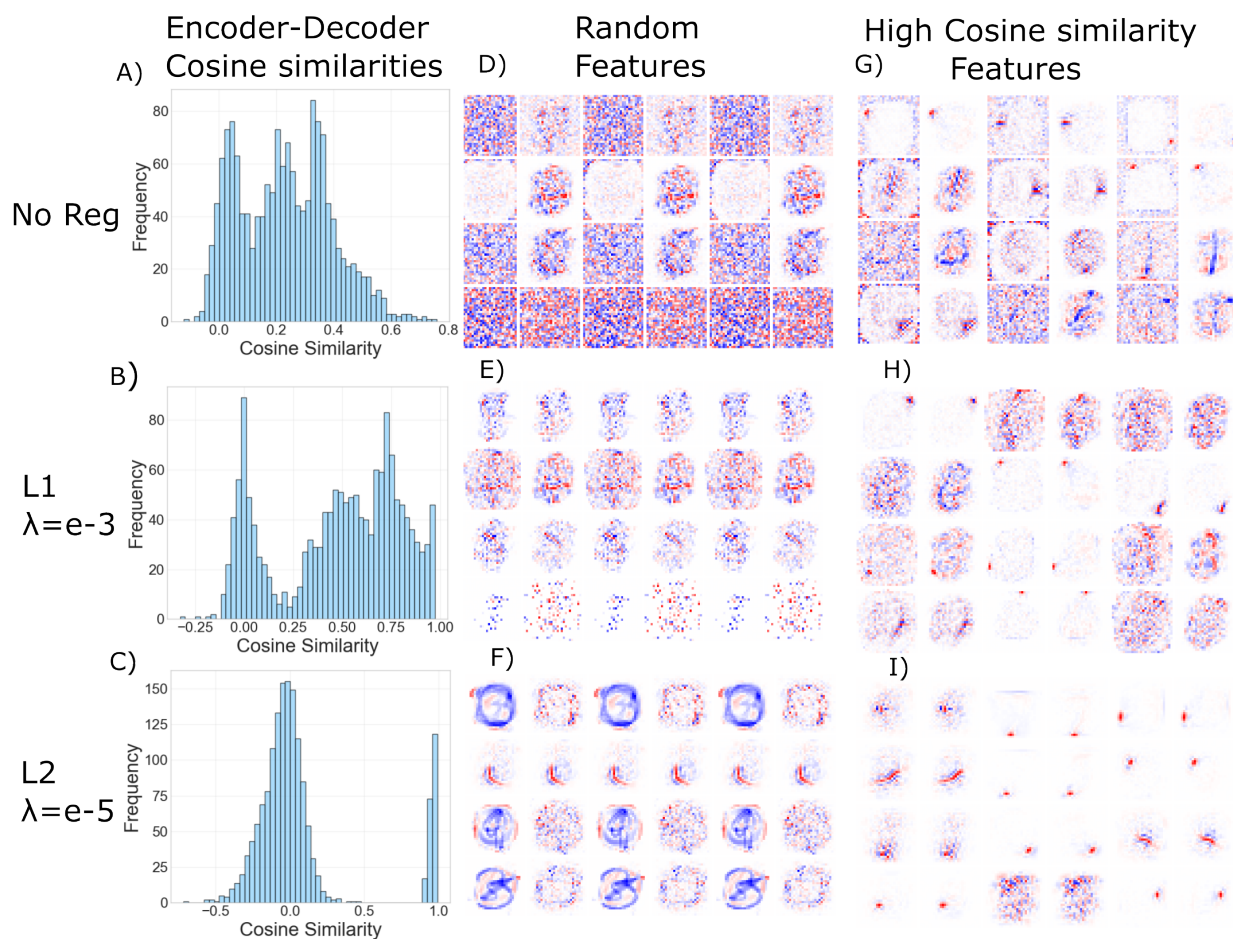


Figure 1: **MNIST cosine similarity and feature visualizations.** **Left column (A–C):** Histograms of encoder–decoder cosine similarity for base, L1, and L2 SAEs (1,568 latents). L2 creates a bimodal distribution with a small high-alignment core. **Right panels (D–I):** Feature pairs showing encoder and decoder (paired next to each other) as  $28 \times 28$  heatmaps (blue = negative, red = positive). Left subcolumns show random samples; right subcolumns show high cosine-similarity features. L2’s high-alignment features capture clean strokes and curves, while the base (no regularization) features appear noisy. The plotted features come from the SAEs without decoder norm constraints.

### 3.2 Regularization improves cross-seed consistency

To match language-model SAE practices, we repeated MNIST training whilst introducing tied initialization and a unit-norm decoder constraint to match the design choices present in SAEBench (Karvonen et al., 2025). Table 1 summarizes cross-seed consistency across three random seeds.

Without decoder constraints and tied initialization, features are mostly not reproducible by the strict shared-feature criterion ( $\approx 0\%$  shared). With tied initialization and unit-norm decoders, adding weight regularization substantially increases the fraction of shared features both for L1 and L2. L2 yields the highest shared-feature fraction for alive features (22.5% vs. 1.9% without regularization). We also observed that shared features appear qualitatively more interpretable than random features when visualized as  $28 \times 28$  heatmaps, capturing strokes and curves, particularly in the encoder weights (Figure 2). Based on these results, we proceeded with SAEBench defaults (tied initialization and unit-norm decoder) for Pythia experiments.

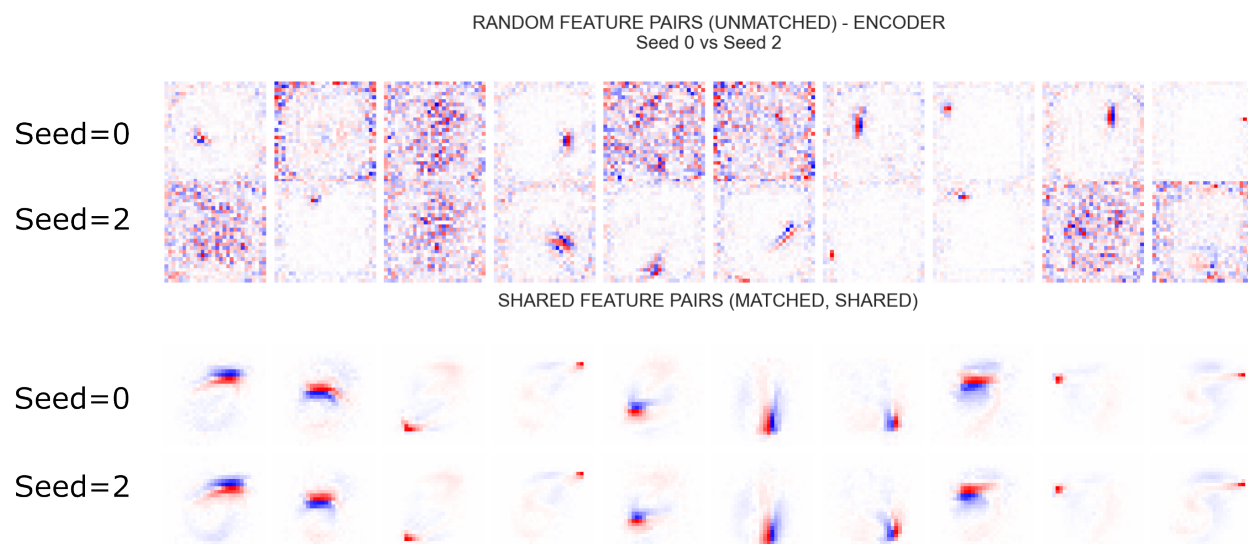


Figure 2: **MNIST shared vs. random feature visualization.** Encoder weights as  $28 \times 28$  heatmaps (blue = negative, red = positive). Top two rows show random features; bottom two rows show features classified as shared between at SAEs with random seed 0 and 2. Each feature scaled to  $\pm \max(|\text{weights}|)$ . Shared features capture clean strokes and curves; random features appear noisy. Features imaged are from the SAE with tied weight and constrained decoder but no weight penalty.

Setting	Weight penalty	Mean max cos	Frac paired ( $> 0.7$ )	Frac shared (All)	Frac shared (Alive)
Untied init	none	0.2400	3.57%	0.00%	0.00%
Tied init (constrained Dec)	none	0.4783	48.28%	1.74%	1.74%
Untied init	L1 ( $\lambda_w = 10^{-3}$ )	0.3260	4.66%	3.21%	0.60%
Tied init (constrained Dec)	L1 ( $\lambda_w = 10^{-3}$ )	0.5486	51.62%	14.07%	14.10%
Untied init	L2 ( $\lambda_w = 10^{-5}$ )	0.5061	7.38%	4.91%	2.90%
Tied init (constrained Dec)	L2 ( $\lambda_w = 10^{-5}$ )	0.3858	42.88%	12.54%	22.50%

Table 1: MNIST cross-seed feature consistency (3 seeds) with unit-norm decoder columns. Weight regularization interacts strongly with decoder constraints and tied initialization (Tied init), L2 regularization increases the fraction of strictly shared features by an order of magnitude.

## 4 Language model experiments

### 4.1 Setup

We evaluated weight regularization on SAEs trained on layer-3 residual stream activations from Pythia-70M-deduped using SAEBench (Karvonen et al., 2025). We tested TopK (Gao et al., 2024), BatchTopK (Bussmann et al., 2024), and Matryoshka (Bussmann et al., 2025) architectures with sweeps over sparsity ( $k \in \{40, 80, 150, 320\}$ ) and regularization strengths ( $\lambda \in \{0, 10^{-12}, 10^{-10}, 10^{-7}, 10^{-5}, 10^{-4}\}$ ), keeping tied initialization and unit-norm decoder columns throughout.

We evaluate on sparse probing (SP), spurious correlation removal (SCR@10), targeted probe perturbation (TPP@10), and CE loss recovery for all architectures. We then measure cross-seed feature sharedness for the TopK architecture, and proceeded with automated interpretability and steering experiments.

### 4.2 SAEBench performance and cosine-similarity structure

Across architectures, weight regularization frequently appears in Pareto-optimal configurations under SAEBench metrics (Appendix D). As in MNIST, TopK models with L2 regularization produce a high-cosine cluster of aligned features alongside many dead latents (Figure 3 and Appendix C). This effect is architecture-dependent: BatchTopK with L2 regularization instead shows a general shift toward lower cosine similarities without the bimodal structure. In TopK models, L2 regularization is particularly aggressive, killing off the majority of features during training (see Appendix C for the full distribution including dead features).

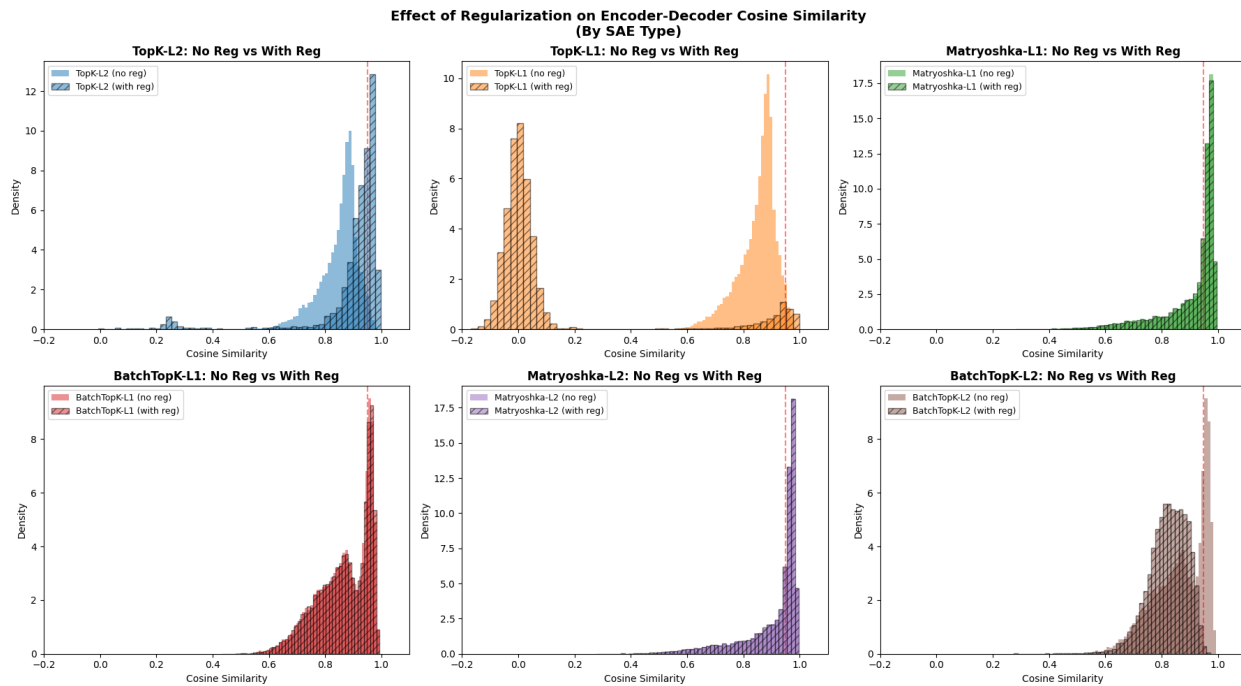


Figure 3: **Encoder-decoder cosine similarity distributions** for regularized (“reg”) vs. unregularized (“no reg”) SAEs across architectures. Dead features (encoder or decoder norm = 0) are excluded; for TopK-L2, the majority of features fall into this category (see Appendix C). The distributions plotted are of the pareto best SAE for each architecture and the not regularized SAE with the corresponding sparsity penalty  $k$ .

### 4.3 L2 regularization increases cross-seed feature sharedness

We computed cross-seed feature reproducibility across three random seeds for TopK SAEs ( $k \in \{40, 80, 150, 320\}$ ), comparing  $\lambda \in \{0, 10^{-4}\}$ . Adding an L2 weight penalty produced a large and consistent improvement across all sparsity levels. The effects are most significant when we filtered the features by removing dead features (cosine similarity of decoder and encoder  $< 0.1$ )(Figure 4): the fraction of strictly shared features among alive features increases over tenfold (from  $< 2\%$  to  $\sim 35\%$ ), mean max cosine similarity among alive features roughly doubles (from  $\leq 0.32$  to  $\sim 0.7$ ), and the fraction of features with cosine similarity  $> 0.7$  in decoder increases almost fivefold (from  $< 10\%$  to  $\sim 50\%$ ).

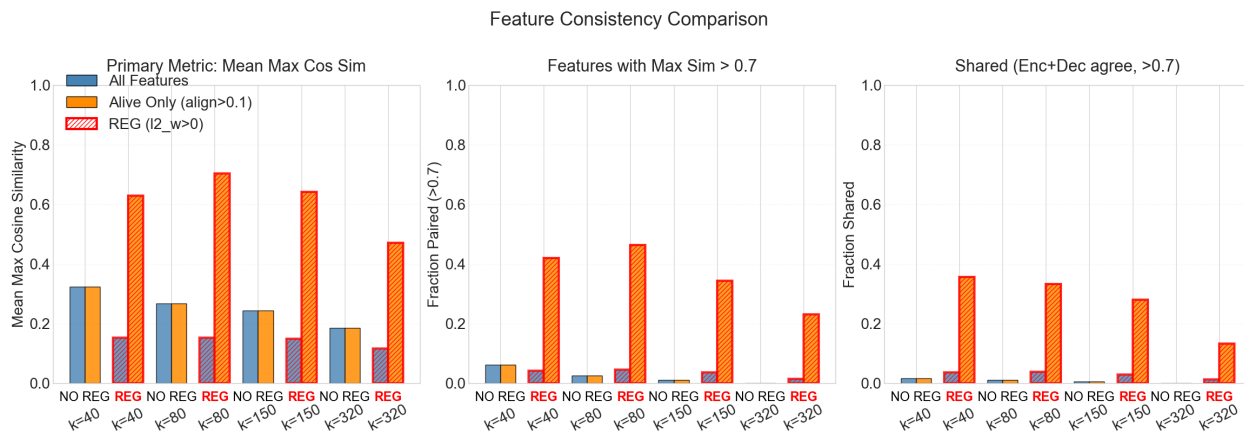


Figure 4: Pythia-70M TopK: cross-seed feature consistency metrics across sparsity levels ( $k$ ) for unregularized (blue) and L2-regularized (orange) SAEs. L2 weight regularization substantially increases sharedness, particularly among alive features (orange bars).

### 4.4 Regularization improves steering and strengthens the auto-interp–steering link

L2 weight regularization improved steering success as sample-level success rates (judge score  $\geq 4$ ) increased from 6.3% (57/900) to 13.0% (72/555;  $\chi^2 = 17.92$ ,  $p < 0.0001$ ). Strikingly, the relationship between auto-interpretability and steering success also strengthens under regularization. The Spearman correlation between auto-interpretability score and per-feature steering success is weak without regularization ( $r = 0.060$ ,  $p = 0.075$ ) but becomes significant with L2 regularization ( $r = 0.144$ ,  $p = 7 \times 10^{-4}$ ). The distribution of auto-interpretability scores themselves remains similar across conditions (Figure 5), suggesting that regularization does not simply improve interpretability scores but instead better aligns what a feature *means* with what it *does*.

**Decoder orthogonality.** To test whether L2 regularization encourages more orthogonal decoder columns, we computed the mean absolute pairwise cosine similarity of the decoder matrix ( $c_{\text{dec}}$ ; (Chanin and Garriga-Alonso, 2025)) for each TopK configuration (Figure 6). Over all features, L2 consistently lowers  $c_{\text{dec}}$ , with the largest reduction at  $k=40$  ( $0.043 \rightarrow 0.036$ ). Though, since L2 kills  $\sim 90\%$  of features, this partly reflects dead-feature dilution. Restricting to alive features reveals a more nuanced picture: at  $k=40$  the values are nearly identical ( $0.043$  vs.  $0.042$ ), while at  $k \geq 80$  the surviving L2 features become progressively *more* orthogonal than the full unregularized dictionary (e.g.,  $0.028$  vs.  $0.035$  at  $k=320$ ). This suggests that at low  $k$ , improved steering may mainly stem from dictionary pruning that reduces off-target interference, whereas at higher  $k$ , regularization produces a genuinely more disentangled feature set.



Figure 5: Pythia-70M TopK  $k=40$ : **(A)** Steering success rate (LLM judge score  $\geq 4$ ); L2 regularization roughly doubles the rate. **(B)** Auto-interpretability score distributions remain similar across conditions. **(C)** Spearman correlation between auto-interpretability and steering success; regularization strengthens the link.

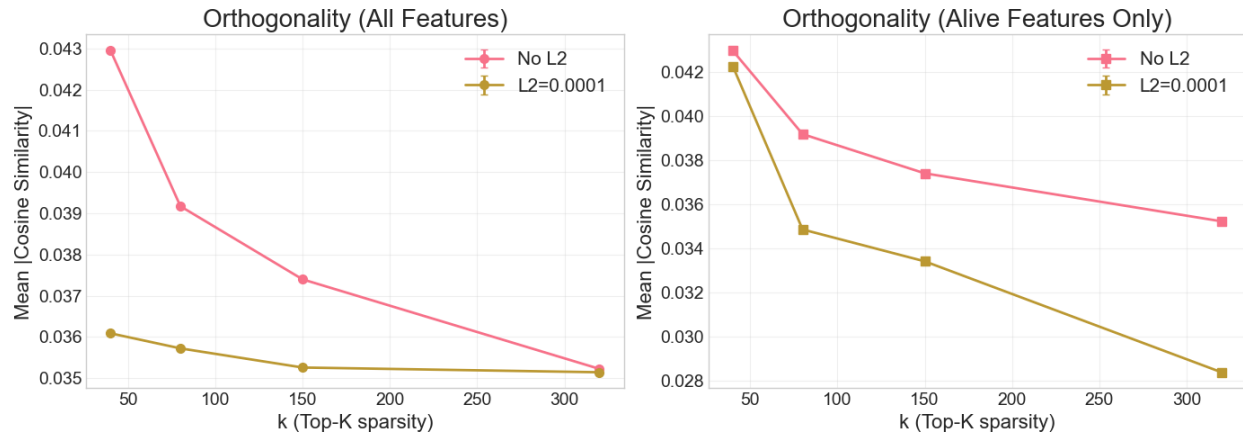


Figure 6: Decoder pairwise cosine similarity ( $c_{\text{dec}}$ ) across TopK sparsity levels (seed 1). **Left:** computed over all features. L2 regularization reduces  $c_{\text{dec}}$ , but this is partly driven by dead features. **Right:** computed over alive features only (encoder–decoder alignment  $> 0.1$ ). At  $k=40$ , alive-feature orthogonality is nearly identical between regularized and unregularized SAEs; at higher  $k$ , the  $\sim 1,000$ – $1,700$  surviving L2 features are *more* orthogonal than the full 16,384-feature unregularized dictionary.

## 5 Discussion

Adding L2 weight regularization to SAE training increases cross-seed feature reproducibility and improves steering success, but arguably at a cost: the majority of latents collapse to zero (Appendix C). This raises the question of whether regularization performs implicit model selection, converging to a low-rank solution that a smaller dictionary could achieve. We believe the answer is partially yes, but the surviving features are not poly-semantic high-variance principal components, rather, their cross-seed alignment and improved steerability suggest they capture functionally meaningful, mono-semantic directions that multiple optimization trajectories independently recover. A natural next step is to compare regularized overcomplete SAEs against smaller unregularized dictionaries matched on alive-feature count. Notably, [Martin-Linares and Ling \(2025\)](#) arrive at a structurally similar outcome through an entirely different mechanism: their attribution-guided distillation of Matryoshka SAEs converges on a core of 197 features (out of 65k) that persist across retraining cycles. That both L2 weight decay and iterative attribution-based pruning dramatically reduce the effective dictionary to a small, high-quality subset suggests that standard SAE dictionaries contain substantial redundancy, and that the “true” number of reliably recoverable features may be far smaller than the nominal dictionary size.

**Interaction with SAE design choices.** Regularization does not act in isolation. In MNIST, the combination of tied initialization, unit-norm decoder columns, and L2 yielded the highest fraction of alive features shared, which is an order of magnitude larger than that of SAE with only regularization or only constraints on the decoder columns (Table 1). The response to regularization is also architecture-dependent: TopK models with L2 produce a bimodal cosine-similarity distribution with a high-alignment core, while BatchTopK instead shows a general shift toward lower similarities without the bimodal structure (Figure 3). Together, these interactions suggest that the effect of weight regularization is shaped by the full training recipe: initialization, decoder constraints, and sparsity mechanism and that exploring combinations of these design choices may yield synergistic improvements.

**Steering and the interp–steering gap.** The roughly doubled steering success rate is practically relevant. We hypothesized that L2 produces decoder columns that are more orthogonal to unrelated directions, reducing off-target effects during activation injection. However measuring decoder pairwise cosine similarity ( $c_{\text{dec}}$ ; [Chanin and Garriga-Alonso, 2025](#)) reveals that among alive features at  $k=40$ , regularized and unregularized SAEs have nearly identical orthogonality (Figure 6). The steering improvement at this sparsity level is therefore better attributed to dictionary pruning: by collapsing  $\sim 90\%$  of latents, L2 removes weakly-used or redundant directions that could otherwise introduce off-target effects during activation injection. At higher  $k$ , however, the surviving features are genuinely more orthogonal than the full unregularized dictionary, suggesting that regularization can produce a more disentangled basis beyond what pruning alone explains. The strengthened correlation between auto-interpretability and steering success (Spearman  $r$ :  $0.060 \rightarrow 0.144$ ) remains notable regardless of mechanism: it indicates that regularization partially closes the gap between what a feature *means* and what it *does*, a decoupling that, when present, is concerning for downstream applications.

A complementary approach is to modify the SAE objective so that learned features are explicitly *functionally important*. [Braun et al. \(2024\)](#) propose end-to-end sparse dictionary learning, training an SAE inserted into a frozen network to minimize the divergence between the original model outputs and the outputs after reconstruction. This directly targets the “what it does” side of the interp–steering gap. Our findings suggest that even a simple L2 weight penalty can partially align textual explanations with controllability. Combining weight regularization with end-to-end, output-preserving objectives might be a promising direction for improving both stability and functional faithfulness.

Improvements in steering reliability are especially relevant for domains where model outputs are not

easily evaluated by humans, such as protein or genomic sequence models. For instance, [Maiwald et al. \(2025\)](#) recently applied SAEs to genomic foundation models and used feature steering to guide generation toward biologically meaningful outputs, a setting where verifying steering fidelity is far harder than in natural language, since neither humans nor language-model judges can readily assess output quality. Consequently, steering experiments must be carefully designed and validated for each feature, making a high proportion of unsteerable features a major practical bottleneck: every unreliable feature wastes laborious validation efforts. Our finding that even simple weight regularization can better align feature explanations with steering behavior suggests it could be a low-cost way to reduce this bottleneck, accelerating the use of mechanistic interpretability for novel scientific discovery with foundation models.

**Connections to prior work.** Our findings connect to a broader question about what makes an SAE solution “correct.” The dead-feature phenomenon we observe can be reinterpreted through the lens of the Minimum Description Length principle ([Ayonrinde et al., 2024](#)): rather than a failure mode, L2 may be eliminating features whose marginal reconstruction contribution does not justify their coding cost, effectively acting as an implicit MDL-like pressure that prunes the dictionary to high-utility features. This interpretation is reinforced by the DMSAE framework ([Martin-Linares and Ling, 2025](#)), whose attribution coverage threshold  $\tau$  serves a functionally similar role: it retains only the smallest feature set whose cumulative contribution to next-token loss reaches a target fraction of the total. Both L2 regularization and attribution-guided selection thus act as complementary forms of complexity control: one operating continuously during optimization, the other applied discretely between training cycles and both converge on compact feature sets with improved downstream properties.

The surviving features we observe are not only more reproducible across seeds but also, at higher sparsity levels, more geometrically disentangled, partially mitigating the non-uniqueness documented by [Gonçalo Paulo and Nora Belrose \(2025\)](#). This regime dependence is notable in light of [Chanin and Garriga-Alonso \(2025\)](#), who show that too-low L0 causes SAEs to mix correlated features into polysemantic latents, detectable via elevated decoder pairwise cosine similarity ( $c_{\text{dec}}$ ). Our measurements (Figure 6) suggest that L2 and sparsity address overlapping but distinct failure modes: at low  $k$ , regularization achieves its benefits primarily through pruning, while at higher  $k$  the surviving features are genuinely more orthogonal than the full unregularized dictionary. Together, these results are consistent with the view that SAE features are decompositions useful for recoding the data into a sparser basis rather than unique ground truths, but that regularization can push the decomposition toward more stable and functionally meaningful directions.

**Limitations and future work.** All language-model experiments use Pythia-70M-deduped; scaling behavior is unknown. Cross-seed and steering analyses focus on TopK, though Figures 3 and Appendix D suggest architecture-dependent responses. Steering evaluation relies on a single LLM judge, and the high dead-feature rate limits applications requiring comprehensive coverage. Key next steps include comparing regularized SAEs against smaller unregularized dictionaries, developing diagnostics that distinguish useful from pathological feature death, exploring regularization annealing schedules, and directly optimizing an MDL-inspired objective during training. A particularly promising direction would be to combine weight regularization with post-hoc feature selection methods such as the attribution-guided distillation of [Martin-Linares and Ling \(2025\)](#): L2 could handle initial pruning and encourage orthogonality during training, while iterative attribution scoring could subsequently identify which surviving features are most functionally important for the base model’s behavior. Both papers also converge on the encoder direction as the primary carrier of feature identity (our L2 pressure is channeled through the encoder by the unit-norm decoder constraint; DMSAEs transfer and freeze only encoder weight vectors), suggesting that future work on feature consistency should focus on the encoder side of the architecture.

## 6 Conclusion

Weight regularization is a simple modification that meaningfully affects SAE behavior. In MNIST, it yields a small aligned core of clean features and under standard training constraints substantially increases cross-seed feature sharedness. In Pythia-70M TopK SAEs, L2 weight regularization increases the fraction of shared features across seeds and improves steering success, while preserving mean auto-interpretability. Regularization also strengthens the relationship between auto-interpretability scores and steering success, suggesting a pathway toward more reliable, functionally meaningful SAE features.

## Acknowledgements

We thank Peter Minary, Craig MacLean and Adam Winnifirth for helpful feedback and discussion. PJ is supported by funding from the Biotechnology and Biological Sciences Research Council UKRI-BBSRC grant (BB/T008784/1). PJ cofounded Evolvere Biosciences, but the company had no role in this study. OMC acknowledges funding from a New College Todd-Bird Junior Research Fellowship and MRC Fellowship MR/Y010078/1. He acknowledges consulting fees to Pelago Biosciences, Faculty.ai and MarketCast and is on the scientific advisory board of Evolvere Biosciences. No funder had a role in the research or decision to publish

## References

- Nelson Elhage, Tristan Hume, Catherine Olsson, Nicholas Schiefer, Tom Henighan, Shauna Kravec, Zac Hatfield-Dodds, Robert Lasenby, Dawn Drain, Carol Chen, Roger Grosse, Sam McCandlish, Jared Kaplan, Dario Amodei, Martin Wattenberg, and Christopher Olah. Toy Models of Superposition. *Transformer Circuits Thread*, 2022. URL [https://transformer-circuits.pub/2022/toy\\_model/index.html](https://transformer-circuits.pub/2022/toy_model/index.html).
- Trenton Bricken, Adly Templeton, Joshua Batson, Brian Chen, Adam Jermyn, Tom Conerly, Nicholas L Turner, Cem Anil, Carson Denison, Amanda Askell, Robert Lasenby, Yifan Wu, Shauna Kravec, Nicholas Schiefer, Tim Maxwell, Nicholas Joseph, Alex Tamkin, Karina Nguyen, Brayden McLean, Josiah E Burke, Tristan Hume, Shan Carter, Tom Henighan, and Chris Olah. Towards Monosemanticity: Decomposing Language Models With Dictionary Learning. 2023. URL <https://transformer-circuits.pub/2023/monosemantic-features/index.html>.
- Hoagy Cunningham, Aidan Ewart, Logan Riggs, Robert Huben, and Lee Sharkey. Sparse Autoencoders Find Highly Interpretable Features in Language Models. 10 2023. URL <http://arxiv.org/abs/2309.08600>.
- David Chanin and Adrià Garriga-Alonso. Sparse but Wrong: Incorrect L0 Leads to Incorrect Features in Sparse Autoencoders. In *Mechanistic Interpretability Workshop at NeurIPS*, 2025. URL <https://github.com/chanind/sparse-but-wrong-paper>.
- Gonçalo Paulo and Nora Belrose. Sparse Autoencoders Trained on the Same Data Learn Different Features. In *39th Conference on Neural Information Processing Systems (NeurIPS 2025) Mechanistic Interpretability Workshop*, 2025. URL <https://arxiv.org/abs/2501.16615>.
- Subhash Kantamneni, Joshua Engels, Senthooan Rajamanoharan, Max Tegmark, and Neel Nanda. Are Sparse Autoencoders Useful? A Case Study in Sparse Probing. 2 2025. URL <http://arxiv.org/abs/2502.16681>.

- Dan Braun, Jordan Taylor, Nicholas Goldowsky-Dill, and Lee Sharkey. Identifying Functionally Important Features with End-to-End Sparse Dictionary Learning. 5 2024. URL <http://arxiv.org/abs/2405.12241>.
- Luke Marks, Alasdair Paren, David Krueger, and Fazl Barez. Enhancing Neural Network Interpretability with Feature-Aligned Sparse Autoencoders. 11 2024. URL <http://arxiv.org/abs/2411.01220>.
- Cristina P. Martin-Linares and Jonathan P. Ling. Attribution-Guided Distillation of Matryoshka Sparse Autoencoders. 12 2025. URL <http://arxiv.org/abs/2512.24975>.
- Ian Goodfellow, Yoshua Bengio, and Aaron Courville. *Deep Learning*. MIT Press, 2016.
- Robert Tibshirani. Regression Shrinkage and Selection via the Lasso. *J. R. Statist. Soc. B*, 58(1):267–288, 1996. URL <https://academic.oup.com/jrsssb/article/58/1/267/7027929>.
- Alex Krizhevsky, Ilya Sutskever, and Geoffrey E Hinton. ImageNet Classification with Deep Convolutional Neural Networks. In *Advances in neural information processing systems*, pages 1097–1105, 2012. URL <http://code.google.com/p/cuda-convnet/>.
- Adam Karvonen, Can Rager, Johnny Lin, Curt Tigges, Joseph Bloom, David Chanin, Yeu-Tong Lau, Eoin Farrell, Callum McDougall, Kola Ayonrinde, Demian Till, Matthew Wearden, Arthur Conmy, Samuel Marks, and Neel Nanda. SAEBench: A Comprehensive Benchmark for Sparse Autoencoders in Language Model Interpretability. In *Proceedings of the 42nd International Conference on Machine Learning*, 6 2025. URL <http://arxiv.org/abs/2503.09532>.
- Leo Gao, Tom Dupré la Tour, Henk Tillman, Gabriel Goh, Rajan Troll, Alec Radford, Ilya Sutskever, Jan Leike, and Jeffrey Wu. Scaling and evaluating sparse autoencoders. 6 2024. URL <http://arxiv.org/abs/2406.04093>.
- Bart Bussmann, Patrick Leask, and Neel Nanda. BatchTopK Sparse Autoencoders. In *Science of Deep Learning Workshop at the 38th Conference on Neural Information Processing Systems (NeurIPS 2024)*., 12 2024. URL <http://arxiv.org/abs/2412.06410>.
- Bart Bussmann, Noa Nabeshima, Adam Karvonen, and Neel Nanda. Learning Multi-Level Features with Matryoshka Sparse Autoencoders. 3 2025. URL <http://arxiv.org/abs/2503.17547>.
- Aaron Maiwald, Piotr Jedryszek, Florent Draye, Garrett M. Morris, and Oliver M. Crook. Decode-gLM: Tools to Interpret, Audit, and Steer Genomic Language Models, 11 2025. URL <http://biorxiv.org/lookup/doi/10.1101/2025.10.31.685860>.
- Kola Ayonrinde, Michael T. Pearce, and Lee Sharkey. Interpretability as Compression: Reconsidering SAE Explanations of Neural Activations with MDL-SAEs. 10 2024. URL <http://arxiv.org/abs/2410.11179>.

## A Steering hyperparameters

We ran a grid search over steering hyperparameters including: (i) deterministic vs. sampling decoding, (ii) applying steering during generation only vs. all forward passes, and (iii) different strength parameterizations (fixed, residual-RMS scaled, target pre-activation delta). Across both regularized and unregularized TopK models, residual-RMS scaling gave the best average LLM-judge score, while fixed-strength steering often gave higher “high-change” rates (fraction of samples with judge score  $\geq 4$ ). The configuration used for the main analyses was non-deterministic decoding (temperature = 0.7, top- $p$  = 0.9) with generation-only steering and fixed scaling ( $\alpha = 5$ ), as it gave the best results for both regularized and unregularized SAEs.

## B MNIST reconstruction MSE ablation

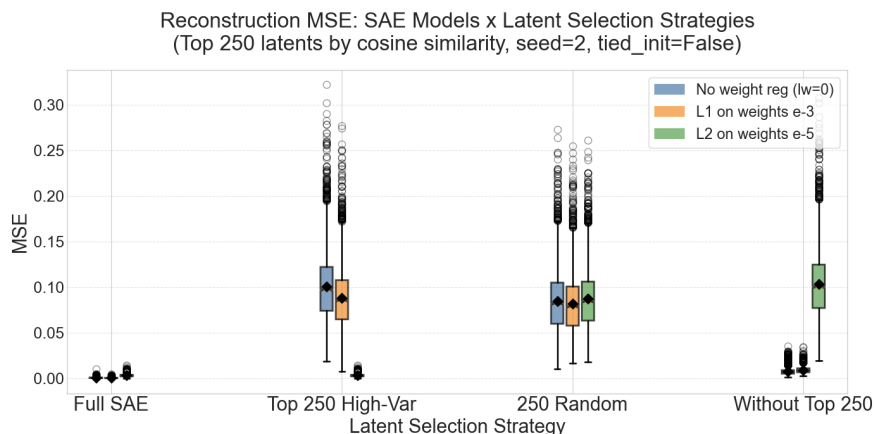


Figure 7: **MNIST reconstruction MSE**. Boxplots measured on the first 250 MNIST examples for three SAE variants (base, L1, L2) under four latent selection strategies: full SAE (all latents active), top-250 high-cosine-similarity latents, 250 random latents, and all latents except the top-250. Top-250 latents were selected per model by sorting on encoder/decoder cosine similarity. A small number of high-cosine similarity latents accounts for most reconstruction capacity in L2-regularized SAEs.

## C TopK-L2 cosine similarity including dead features

## Cosine Similarity Distribution Including Dead Features (Zero)

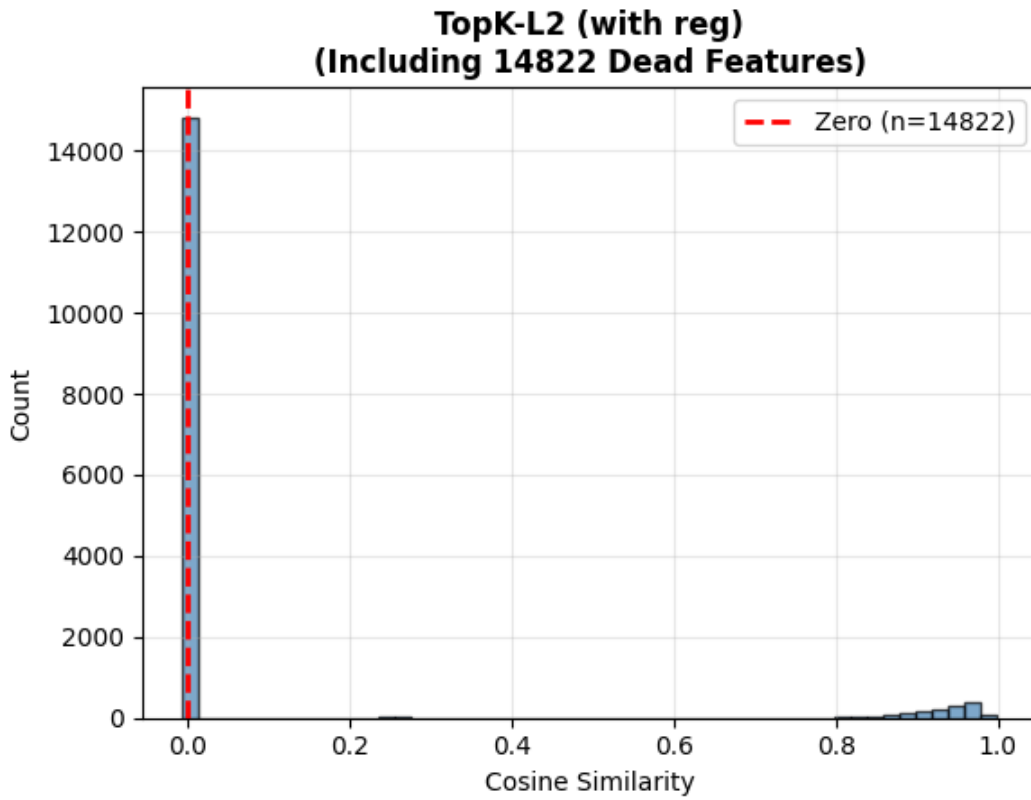


Figure 8: **TopK cosine similarity including dead features.** Encoder–decoder cosine similarity distributions for regularized vs. unregularized TopK SAEs, retaining features where the encoder or decoder norm is zero. The majority of L2-regularized features collapse to zero norm during training.

## D SAEBench Pareto analysis

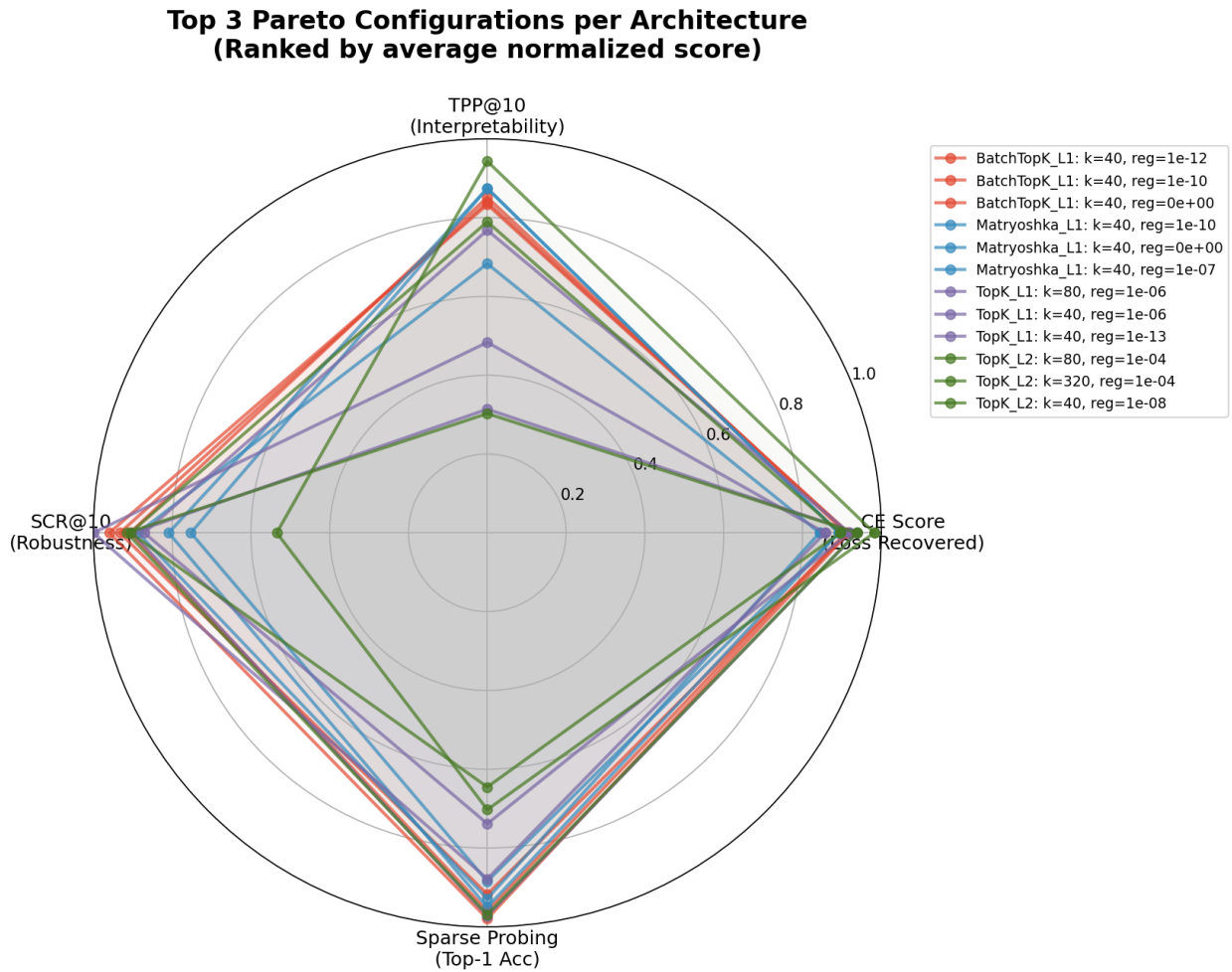


Figure 9: **SAEBench Pareto analysis.** Aggregated top-3 Pareto configurations per architecture. Regularized models frequently appear on the Pareto frontier. Radar plots showing normalized SAEBench metrics for hyperparameter sweeps. Red = Pareto-optimal; gray = dominated. Axes: TPP@10, CE score, SCR@10, SP Top-1 (higher = better).